IEEE Access
Multidisciplinary | Rapid Review | Open Access Journal

Received April 6, 2022, accepted May 9, 2022, date of publication May 13, 2022, date of current version May 19, 2022.

Digital Object Identifier 10.1109/ACCESS.2022.3174958

Phasor Modeling Approaches and Simulation Guidelines of Voltage-Source Converters in Grid-Integration Studies

VINÍCIUS A. LACERDA, EDUARDO PRIETO ARAUJO, (Senior Member, IEEE), MARC CHEAH-MAÑE, (Member, IEEE), AND ORIOL GOMIS-BELLMUNT, (Fellow, IEEE)
Centre d'Innovacio Tecnològica en Convertidors Estatics i Accionaments, Universitat Politècnica de Catalunya (CITCEA-UPC), 08034 Barcelona, Spain

Corresponding author: Vinícius A. Lacerda (vinicius.lacerda@upc.edu)

This work was supported by the European Union's Horizon 2020 Research and Innovation Program [Powering System Flexibility in the Future through Renewable Energy Sources (POSYTYF) Project] under Grant 883985. The work of Oriol Gomis-Bellmunt was supported by the Institució Catalana de Recerca i Estudis Avançats (ICREA) Academia Program.

ABSTRACT With the large integration of converter-interfaced generation (CIG) and widespread of power electronic interfaced technologies, power system dynamic behaviour is becoming progressively faster. As a consequence, is often unclear when to use EMT or Phasor models in grid integration studies. Therefore, this paper presents useful simulation guidelines of Voltage-Source Converters (VSCs) used in AC grid integration studies. It also presents several EMT and Phasor models suited to simulate CIG and renewable energy resources connected to power systems. Several modelling approaches and suitability analyses were provided based on a comprehensive comparative study among the models. Various studies were performed in a small system, composed of two generators, and a CIGRE benchmark system, both modelled in Simulink. We address a gap related to the suitability of CIGs phasor models in studies where the boundary between electromagnetic and electromechanical transients overlap. An insightful analysis of the adequate simulation time step for each model and study is also provided.

INDEX TERMS Converter-interfaced generation (CIG), grid-integration studies, inverter-based resource (IBR), phasor model, simulation, voltage-source converter (VSC).

I. INTRODUCTION

In power system studies, it is common to make simplifying assumptions to simulate systems in a limited computation time. In the past, the boundary between electromagnetic and electromechanical studies was clear, facilitating the use of these assumptions [1]. However, with the large integration of converter-interfaced generation (CIG) and widespread of power electronics-interfaced technologies, power system dynamic behaviour is becoming progressively faster, making both modelling approaches to overlap [2]. In this context, it is often unclear when it is appropriate to use Electromagnetic Transient (EMT), Phasor Model (PM) or other alternative simulation methods.

The significant research activity into the control and stability of power systems with large penetration of CIGs and HVDC systems is fostering the search for new simulation methods. The challenge is to have a sufficiently accurate model to capture the fast dynamics of power electronics, but not computation-intensive to enable simulating large systems. One research area focus on new modelling methods such as Dynamic Phasors [3]–[5], Harmonic State-Space modelling [6]–[10], Harmonic Phasor Domain [11] and frequency-dependent equivalents [12], [13], that aim to model more precisely the fast dynamics of power electronics but keeping the computational cost lower than in EMT. Another research area focuses on co-simulation methods [14]–[17], where the power grid is often modelled in PM or another low-frequency equivalent model while the converter or power electronics device is modelled in EMT. Moreover, DC-side dynamics have also being studied using linearized and generalized models [18]–[20].

However, little research has been conducted on the capabilities of full PM models to perform CIG integration studies (such as stability, protection and control) when the boundary between electromagnetic and electromechanical

The associate editor coordinating the review of this manuscript and approving it for publication was Siqi Bu.

This work is licensed under a Creative Commons Attribution 4.0 License. For more information, see https://creativecommons.org/licenses/by/4.0/

domains overlap. While important recommendations and guidelines were recently available [21], [22], those are often high-level and based on the researchers' experience. Moreover, important questions still need to be addressed, such as the maximum simulation time step for each study, the use of PM models in short-circuit studies and the influence of harmonics in PM simulation.

Therefore, this paper presents several models that can be used to simulate CIG based on Voltage-Source Converters (VSC). It also analyses the suitability of PM models to several power system studies and provides simulation guidelines based on a comprehensive comparative study of EMT and PM models. The paper is organized as follows. Section II introduces the conventional VSC modelling in EMT. Section III briefly describes phasor simulation and approximated VSC phasor models. Section IV presents the methodology to conduct the comparative analysis, including the systems simulated and the tests performed. The results are shown in Section V along with specific discussions. General discussions and simulation guidelines are provided in Section VI. Finally, the conclusions are drawn in Section VII.

II. VSC EMT SIMULATION

Several simulation models of VSC were proposed, varying from detailed models, in the semiconductors domain, to high-level RMS models used in power flow and system planning studies [23], [24]. The proper choice will depend on the level of detail, the phenomena being analysed, and the time available for simulation. Three common types of VSC models are the switching model (SW), the average value model (AVG) and the PM. The AVG model neglects the converter's high-frequency switching and considers that the VSC output voltage is a linearly amplified form of the modulation index, which is nearly sinusoidal [25]. Thus, the VSC electrical model on the AC side is simply a controlled voltage source. As a result, the AVG model focuses only on the power frequency component, which effectively exchanges power with the grid.

A. CONTROL SYSTEM

The modulation index is defined by a control system. In this study, a classic hierarchical structure is presented. The inner loop regulates the positive and negative sequence output current in the *dq* frame using the double synchronous reference frame (DSRF) [26]. The outer loop regulates the AC power injected into the grid. Proportional-integral controllers (PI) of the form $G(s) = k_p(1 + 1/(\tau_i s))$ are used in both loops.

The dynamic behaviour of the converter's output current in the *abc* frame (i_c^{abc}) is expressed as

$$v_c^{abc} - v_g^{abc} = Ri_c^{abc} + L\frac{\mathrm{d}}{\mathrm{d}t}i_c^{abc} \tag{1}$$

where v_c^{abc} is the converter output voltage, v_g^{abc} is the grid voltage and R and L are the equivalent resistance and inductance from the converter to the point of common coupling, respectively, as shown in Fig. 1.

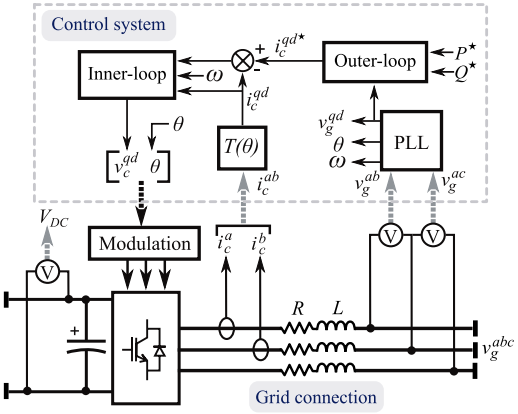

FIGURE 1. VSC diagram.

Transforming (1) to the *dq* frame yields

$$v_c^{qd} - v_g^{qd} = \begin{bmatrix} R & L\dot{\theta} \\ -L\dot{\theta} & R \end{bmatrix} i_c^{qd} + L\frac{\mathrm{d}}{\mathrm{d}t}i_c^{qd} \tag{2}$$

where $\dot{\theta}$ is the voltage phase time derivative (grid instantaneous angular frequency) and it is used in the Park transform to produce constant voltages and currents in the *dq* frame.

The synchronized θ is obtained from the Phase-locked Loop (PLL), aligned with v_q such that $v_d = 0$. Several PLL implementations have been proposed in the recent years [27]. In this study, the conventional synchronous reference frame PLL (SRF-PLL) [27] and tuning approach proposed by [28] was used. The PLL gains were

$$\zeta_{pll} = 1/\sqrt{2} \tag{3}$$
$$k_{p,pll} = 2\zeta_{pll}\omega_{pll}/V_{g,pk} \tag{4}$$
$$\tau_{i,pll} = 2\zeta_{pll}/\omega_{pll} \tag{5}$$

where ζ_{pll} is the damping factor, $k_{p,pll}$ is the proportional gain, $\tau_{i,pll}$ is the integral time constant and $V_{g,pk}$ is the grid phase-to-ground peak voltage.

The inner-loop PI controller gains were tuned using the internal model control approach [29], yielding

$$\tau_{i,c} = L/R \tag{6}$$
$$k_{p,c} = L\omega_c \tag{7}$$

where ω_c is the desired closed-loop bandwidth, $k_{p,c}$ is the proportional gain and $\tau_{i,c}$ is the integral time constant.

The outer-loop PI controllers are identical for both active and reactive power control, with gains tuned according to the modulus optimum criteria [30], yielding

$$\tau_{i,pq} = 1/\omega_c \tag{8}$$
$$k_{p,pq} = \tau_{i,pq}\omega_{pq}\, 2/(3V_{g,pk}) \tag{9}$$

where ω_{pq} is the desired closed-loop bandwidth, $k_{p,pq}$ is the proportional gain and $\tau_{i,pq}$ is the integral time constant.

1) FREQUENCY DROOP

The conventional frequency droop without deadband was implemented, where the additional active power injected by the VSC into the grid (ΔP) is proportional ($k_{droop,f}$) to the frequency deviation (Δf):

$$\Delta P = \Delta f / k_{droop,f} \tag{10}$$

where Δf is obtained by low-pass filtering $\dot{\theta}$, which is estimated by the PLL.

2) VOLTAGE DROOP

Similarly, the conventional voltage droop is implemented, where the additional reactive power injected by the VSC into the grid (ΔQ) is proportional ($k_{droop,v}$) to the voltage deviation ($\Delta|v|$):

$$\Delta Q = \Delta|v| / k_{droop,v} \tag{11}$$

where $\Delta|v|$ is obtained by low-pass filtering v_g^q.

3) LOW VOLTAGE RIDE THROUGH (LVRT)

When the grid voltage drops below a minimum ($v_{g,min}$), the VSC is often required to inject reactive current to support the grid. This characteristic is implemented following a LVRT curve, where the reactive current reference is defined by

$$i_c^{d\star} = k_{lvrt}(v_{g,min} - v_g^q) \tag{12}$$

When the LVRT characteristic is activated, the current reference $i_c^{d\star}$ is defined only by the LVRT characteristic and not by the reactive power control loop, to avoid incurring in two conflicting control objectives. $i_c^{d\star}$ is saturated if exceeds the limit $i_{lvrt,max}$, which is a parameter of the LVRT characteristic.

4) NEGATIVE SEQUENCE CONTROL

A sequence extraction technique is required to implement the DSRF, which can be performed by notch or high-pass filtering, or signal cancellation techniques. In this study, the Delayed Signal Cancellation (DSC) method [31] was used due to its simplicity, despite its non-ideal performance during off-nominal grid conditions. As both positive and negative sequence components were available, the control approach adopted was to have the PLL aligned with the positive sequence voltage (v_g^{q+}) and to define negative sequence current references $i_c^{q-\star} = 0$ and $i_c^{d-\star} = 0$.

III. PHASOR SIMULATION

In typical transient stability studies, it is assumed that the power system frequency remains close to the nominal value (50 Hz or 60 Hz). Thus, phasor simulation aims to capture only the slow dynamics of the power grids, such as the electromechanical transients, with time constants generally bigger than 100 ms. In this mode, the grid differential equations resulting from the interaction of RLC elements are substituted by algebraic equations. Also, the distributed models of transmission lines and cables are substituted by lumped models, based on equivalent impedances. Thus, the system voltages and currents are given by

$$\mathbf{V} = \mathbf{ZI} \tag{13}$$

where $\mathbf{V}$ and $\mathbf{I}$ are the complex-valued vectors of node voltages and current injections, and $\mathbf{Z}$ is the impedance matrix.

As the phasors are assumed to be rotating at nominal angular speed, voltages and currents have their dynamics around 0 Hz. This allows to dramatically increase the simulation time step and consequentially the simulation speed. Depending on the time step used and on the phenomena being simulated, the simulation speed can be increased in one to three orders of magnitude compared to detailed EMT simulation, which is especially interesting when simulating large networks for long periods. However, the speed-up provided by PMs must be used with care because several EMT phenomena are entirely neglected in phasor simulation, which can result in overestimated or underestimated values.

In phasor simulation, the VSCs are represented as current sources with magnitude and angle defined by the control system, as depicted in Fig. 2. Using current sources provided a more stable simulation in Simulink than using voltage sources. As phasor simulation aims mainly to speed up and simplify simulations, several approximations can be performed in the VSC control system to allow larger simulation time steps. In this study, four approaches were compared, which are described next and summarized in Fig. 2.

The conventional VSC model is composed of five parts: the electrical part, the transformation from *abc* to *dq*, the outer control loop, the inner control loop and the transformation from *dq* to *abc*. The electrical part and the transformation from *abc* to *dq* frame are the same amongst all phasor models. As in phasor simulation the voltage phase is readily available, no PLL is needed. To have $v_d^+ = 0$ as in EMT, is only necessary to take the angle (θ) of the grid positive sequence voltage and rotate the voltages and currents in the *abc* frame with respect to this angle. Positive and negative sequences are calculated using Fortescue's theorem. Conversely, opposite rotation is performed when transforming from the *dq* frame to the *abc* frame before sending the reference to the current source.

A. PHASOR MODEL FULL

In this model, the VSC inner and outer control loops are exactly the same as those used in EMT. Thus, it completely represents the dynamics of the control system. As the output of the inner control is the reference voltage and the electrical part is a current source, the reference voltage is transformed in reference current using the electrical dynamics up to the point where the voltage is being measured. This approach provide a smooth transition from voltage to current reference and has the additional benefit of modelling the dynamics of the AC side connection, which is normally neglected in phasor simulation. In this study, an RL filter was used, so the dynamics of the positive and negative-sequence currents

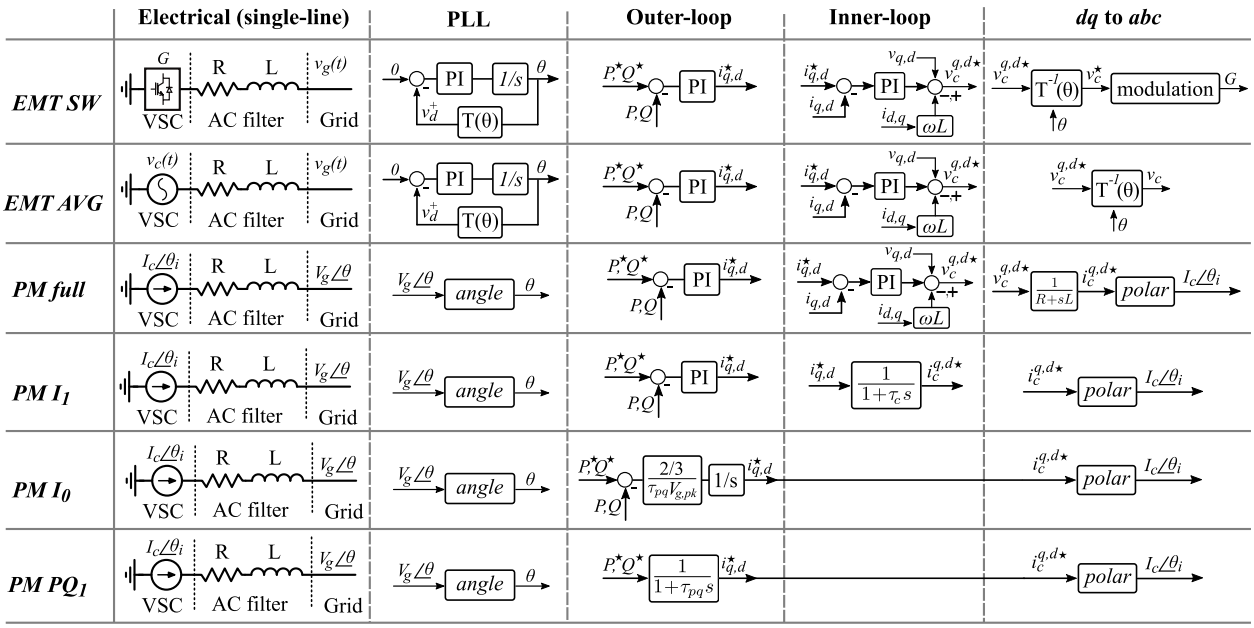

FIGURE 2. Summary of VSC EMT and PM models.

(I_c^{dq+} and I_c^{dq-}) are the ones described by the Laplace transform of (2), as follows

$$I_c^{d+\star} = (v_g^{d+} - v_c^{d+\star} + \omega_g L I_c^{q+})/(R + sL) \quad (14)$$

$$I_c^{q+\star} = (v_g^{q+} - v_c^{q+\star} - \omega_g L I_c^{d+})/(R + sL) \quad (15)$$

$$I_c^{d-\star} = (v_g^{d-} - v_c^{d-\star} - \omega_g L I_c^{q-})/(R + sL) \quad (16)$$

$$I_c^{q-\star} = (v_g^{q-} - v_c^{q-\star} + \omega_g L I_c^{d-})/(R + sL) \quad (17)$$

where superscript $\star$ means the reference signal and ω_g is the grid frequency. Using this approach, the complete control structure used in EMT simulations is preserved (see Fig. 2), which facilitates comparison between PM and EMT.

B. PHASOR MODEL I_1

In this model, the VSC inner control is substituted by a first order transfer function with time constant τ_c, defined to match the original closed-loop bandwidth:

$$\tau_c = \frac{1}{\omega_c} \quad (18)$$

With this approximation, the DSRF closed-control structure is removed, including the cross-coupling term $\omega_g L$. As a consequence, the inner-loop output becomes the low-pass filtered (τ_c) current reference defined by the outer-loop control, which is transformed to the *abc* frame and sent to the current source.

C. PHASOR MODEL I_0

In this model, the VSC inner control is completely removed. As the inner control is the fastest dynamics of the VSC (when neglecting the switching), removing this loop allows bigger time steps to be used, which greatly speeds up simulations. However, it neglects completely the dynamics of the current-control. Thus, this model should be used in studies where these dynamics are not especially relevant.

Moreover, neglecting the time constant of the inner loop also affects the total (inner + outer) closed-loop response. To maintain the new closed-loop time constant equal to the original closed-loop time constant we define:

$$C_{pq}(s) = \frac{G_{pq}(s)}{1 + G_{pq}(s)} = \frac{1}{1 + \tau_{pq} s} \quad (19)$$

where $\tau_{pq} = 1/\omega_{pq}$ is the original closed-loop time constant in (9), $C_{pq}(s)$ is the new close-loop transfer function and $G_{pq}(s)$ is the new open-loop transfer function, defined as

$$G_{pq}(s) = K_{pq}(s)\frac{3}{2}v_g^q \quad (20)$$

where $K_{pq}(s)$ is the new controller transfer function. Solving (19) for $K_{pq}(s)$ yields:

$$K_{pq}(s) = \frac{2}{3v_g^q}\frac{1}{\tau_{pq} s} \quad (21)$$

Thus, to have the same time constant, the original PI controller is substituted by an integrator with a gain equal to $2/(3v_g^q \tau_{pq})$. As v_g^q is variable, it is often useful to consider a static gain by using $V_{g,pk} \approx v_g^q$. Note that in this structure, the signal sent to the integrator is the error between the reference and the measured power output, hence a closed-loop.

D. PHASOR MODEL PQ_1

Further simplification can be achieved if the outer-loop is substituted by a first-order transfer function with the same time constant (τ_{pq}) as the original loop, similar to PM I_1.

With this approximation, the outer loop becomes an open-loop where the output current reference is defined by

$$i^{q+\star} = \frac{2}{3}\frac{P^\star}{v_g^{q+}}, \quad i^{d+\star} = \frac{2}{3}\frac{Q^\star}{v_g^{q+}} \tag{22}$$

where $P^\star$ and $Q^\star$ are the active and reactive power references, respectively.

Next, the tests performed to assess the VSC models are described, followed by a discussion about their suitability.

IV. METHODOLOGY

In order to assess the aforementioned models, various studies were performed in a small system and a CIGRE benchmark HV system, modelled in Simulink. The small system was composed of a synchronous generator, a transmission line and a VSC. The CIGRE system was composed of four synchronous generators, eight transmission lines and two VSCs. The CIGRE system was based on the European HV transmission system in [32], with a few adaptations. Both systems were simulated using a fixed time step and the Euler method (algorithm *ode1* in Matlab). The single-line diagrams of the both systems are depicted in Fig. 3 and Fig. 4, and their parameters are summarized in Table 2, in the Appendix.

For all tests, the EMT AVG model running at 5 μs was defined as the reference model, while the phasor models and the AVG EMT model running at bigger time steps were compared against the reference model. The EMT SW model was not used as the reference model because the high frequency components present in the currents and voltages would equally increase the RMSE in all models, thus precluding a precise comparison among them.

Three key aspects were analysed for each model: i) Precision, ii) Minimum simulation time step and iii) Total execution time.

The precision was quantified using the Root-Mean-Square Error (RMSE) between the variables simulated using each model and the variables simulated using the reference model:

$$RMSE = \sqrt{\frac{1}{N}\sum_{k=1}^{N}\left(x_{ref}(k) - \hat{x}(k)\right)^2} \tag{23}$$

where k is the sample, N is the time window length, x_{ref} is a variable in the reference model and $\hat{x}$ is the same variable in the model being assessed. In this study, the RMSE was divided by a proper base in each study, to present the results in a meaningful scale.

The minimum simulation time step was defined as the time step necessary to capture all the system dynamics and phenomena being analysed, which was assessed using the precision.

The total execution time was defined as the time necessary to run each study.

Table 1 summarizes the tests performed in both systems.

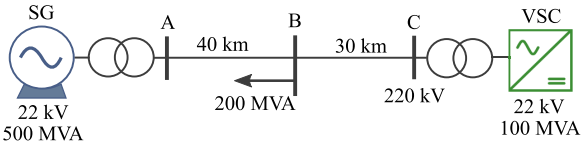

FIGURE 3. Small system single-line diagram.

TABLE 1. Tests performed.

	Small system	CIGRE system	Variables
Setpoint tracking	•		P_{ac}, i_{dq}
Harmonics	•		i_{dq}, v_{dq}
Frequency/Voltage deviation	•		f,V_{abc}
Symmetrical faults	•		$i_{dq}, v_{dq}, T_e, \omega_m$
Asymmetrical faults	•	•	$i_{dq}, v_{dq}, T_e, \omega_m$
Loss of generation		•	$i_{dq}, v_{dq}, T_e, \omega_m$
Line outage		•	$i_{dq}, v_{dq}, T_e, \omega_m$
Simulation time steps	from 5 μs to 12000 μs		

V. SIMULATION RESULTS

This section presents the simulation results, followed by brief discussions. Due to the extensive number of tests, only a portion of the cases and variables are presented, which are representative of each test.

A. SMALL SYSTEM

1) SETPOINT TRACKING

In this test, active and reactive power setpoints were set to 50 MW and 30 Mvar at $t = 0.6$ s and $t = 0.8$ s, respectively. Negative-sequence control and LVRT were disabled during this test, as well as frequency and voltage droop. Fig. 5 presents the converter currents for all models with a time step of 25 μs, 250 μs and 2500 μs, respectively.

As can be observed, for smaller time steps, both EMT and PM models presented very similar results. However, as the simulation time step increases, the models that represent faster dynamics starts to deviate from the reference until they completely diverge. This can be better visualized by varying the simulation time step between 5 μs and 12000 μs, as shown in Fig. 6.

As can be observed in this test, the PM PQ_1 model is worse than the other models for small time steps but its precision gets similar to the others for bigger time steps. Although the PM I_1 and I_0 approximate or neglect the current loop, they presented low error because their dynamics are smoothed by the outer loop, which is slower.

When the simulation time step gets closer to the model's fastest dynamics, the error increases dramatically. In the system of Fig. 3, the fastest dynamics are related to the VSC current control loop, which have a time constant equal to $1/\omega_c = 1.18$ ms. This is evident in Fig. 7a that shows the *PM full* model error for several current control bandwidths. As the bandwidth increases, the maximum simulation time step to achieve low errors reduces proportionally. However, much higher time steps can be used (Fig. 7b) when performing the

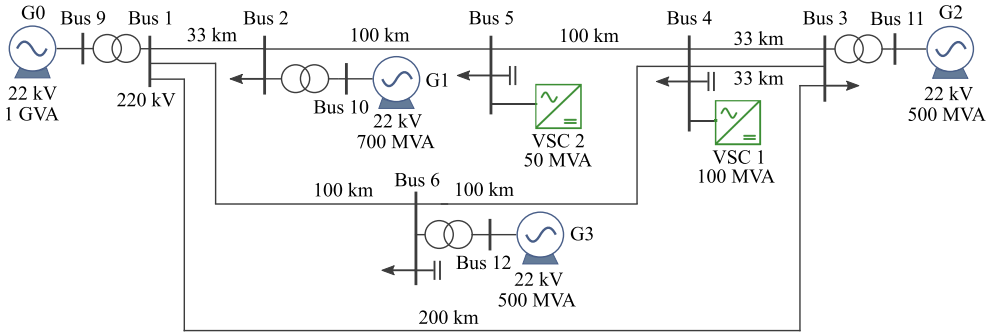

FIGURE 4. CIGRE system single-line diagram. Modified from [32].

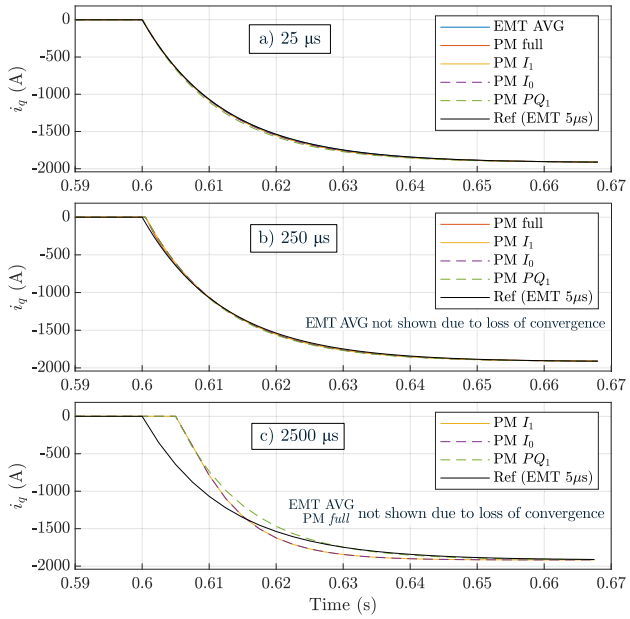

FIGURE 5. Test 1 – i^{q+} setpoint tracking simulated by each model at a) 25 μs, b) 250 μs and c) 2500 μs.

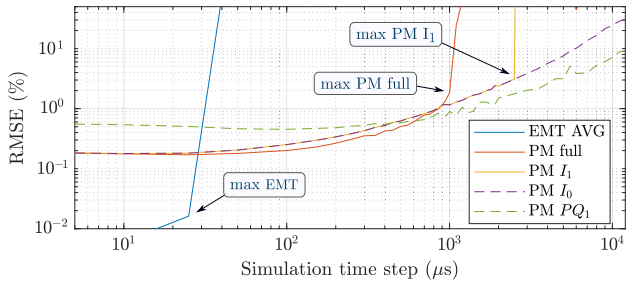

FIGURE 6. Test 1 – P_{ac} setpoint tracking simulated by EMT and PM models RMSE for several simulation time steps.

same test with the *PM* I_0 model as it neglects the current control loop and the fastest dynamics becomes the outer loop.

2) FREQUENCY/VOLTAGE DEVIATION

In this test, an additional 150 MW, 20 Mvar constant impedance load was connected to bus B at $t = 1\,s$, dropping

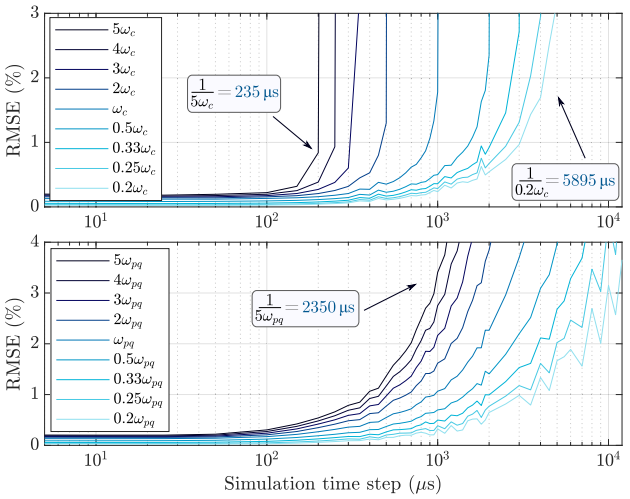

FIGURE 7. Test 1 – P_{ac} RMSE for several time steps and power control bandwidths. a) *PM full* and b) *PM* I_0 model.

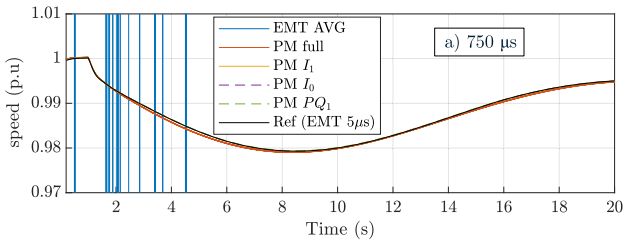

FIGURE 8. Test 2 – ω_m simulated by each model at 750 μs.

the system frequency to around 49 Hz. The VSC frequency and voltage droops were enabled during this test.

As this test has slower dynamics, a few differences were observed between EMT and PM models, as can be observed in the synchronous generator (SG) speed in Fig. 8. The EMT AVG diverged due to numerical instability resulting from the large simulation step used. Moreover, faster dynamics are mechanically "low pass filtered" due to the generators inertia, which explains why the SG speed matches accurately even thought the electrical torque is oscillatory in EMT and constant in PM, as shown in Fig. 9.

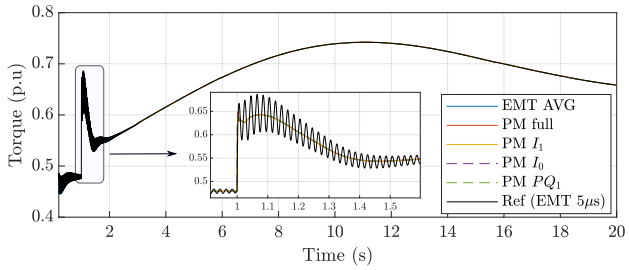

FIGURE 9. Test 2 – *Te* simulated by each model at 25 μs.

The total execution time for each time step is shown in Fig. 10. As can be observed in Fig. 10, there is an inverse relationship between time step and execution time. Thus, choosing a proper time step can greatly reduce the execution time without any change in the model.

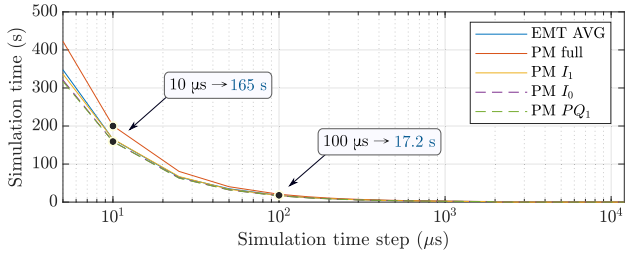

FIGURE 10. EMT and PM models simulation times for several time steps.

3) SYMMETRICAL FAULT

In this test, a 7 Ω three-phase fault was applied to bus B at $t = 2.5\,s$, lasting for 300 ms. The LVRT was enabled during this test.

Fig. 11 shows the current at phase B. As can be observed in Fig. 11, PM models matched the EMT model closely in steady-state. After the transient, the PM models took only a few cycles to match the EMT model, similar to the time the PLL took to track the reference in Fig. 12. The PM PQ_1 showed a slightly bigger deviation at $t = 2.8$ s in Fig. 12 because as it has no PI controller in the outer loop, no saturation effects could be implemented, making the VSC to inject more power just after the transient. This also affected the generator's speed, showed in Fig. 13. The tiny spike at $t = 2.95$ in Fig. 12 was numerical, due to the high time-step used in this test.

4) ASYMMETRICAL FAULT

In this test, a 10 Ω single-phase fault at phase B was applied to bus B at $t = 2.5\,s$, lasting for 300 ms. The negative-sequence control was enabled during this test.

Fig. 14 shows the current at phase B. Comparing Fig. 14 with Fig. 11 it can be observed that PM models presented a slightly higher error in the current magnitude for asymmetric faults, which were observed during the whole fault period, differently from the error in the symmetrical fault that reduced after 100 ms.

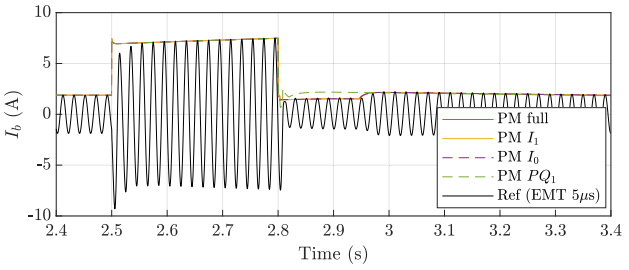

FIGURE 11. Test 3 – I_b simulated by each model at 350 μs.

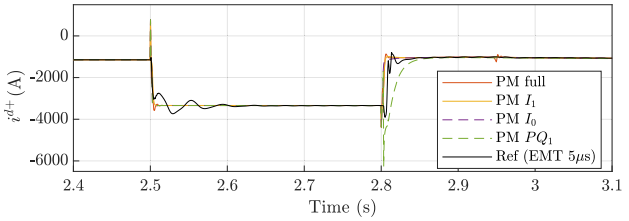

FIGURE 12. Test 3 – i^{d+} simulated by each model at 600 μs.

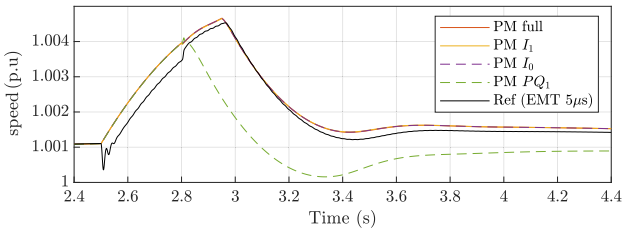

FIGURE 13. Test 3 – ω_m simulated by each model at 600 μs.

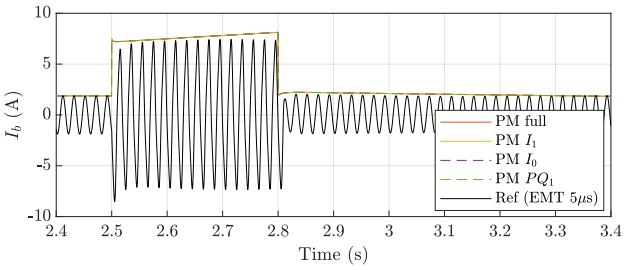

FIGURE 14. Test 4 – I_b simulated by each model at 350 μs.

During an asymmetric fault, EMT models show an oscillatory torque produced by the transient, which only the average value is captured by the PM models, as shown in Fig. 15. Despite the higher error during the transient, the PM models match the EMT model closely after less than a second.

As the strategy adopted for negative sequence control was $i_c^{q-\star} = 0$ and $i_c^{d-\star} = 0$, these variables were controlled to zero even during the transient in the PM models, as shown in Fig. 16. The results with the PM models were more optimistic than the ones with EMT because the symmetric components in PM models are already available and do not need to be estimated as in EMT. This avoids the transient seen in Fig. 16 after the beginning and the end of the fault and also avoids any delay in the sequence estimation, while this delay is

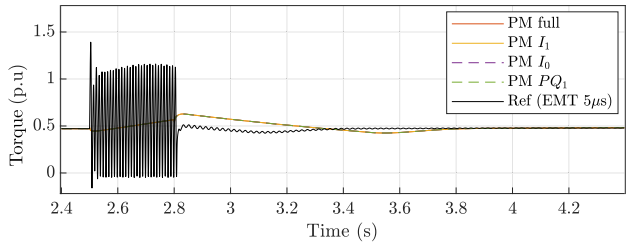

FIGURE 15. Test 4 – T_e simulated by each model at 350 μs.

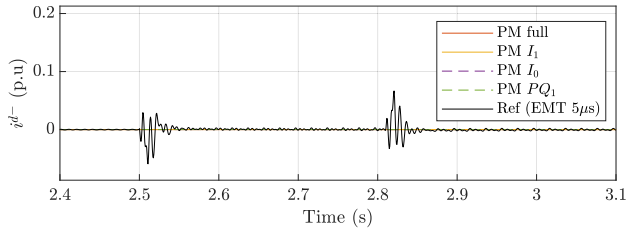

FIGURE 16. Test 4 – i^{d-} simulated by each model at 600 μs.

intrinsic in the DSC in EMT [31] or in any other filtering-based method.

5) HARMONICS

In this test, a predefined harmonic content was injected into the system using harmonic current sources at $t = 0.5\,s$, and at $t = 0.6$ s the VSC active power setpoint was set to 50 MW. The harmonic orders were 2, 3, 4, 5, 7, 11 and 13, with magnitudes 1%, 25%, 2.5%, 15%, 7.5%, 4% and 2.5%, respectively, with reference to a 30 MW, 10 MVar load.

Fig. 17 presents v_{q+} measured at the converter's terminal after the injection of the harmonic components. As can be observed, the PM models, though not matching the EMT model, also revealed the harmonic corruption in the voltage.

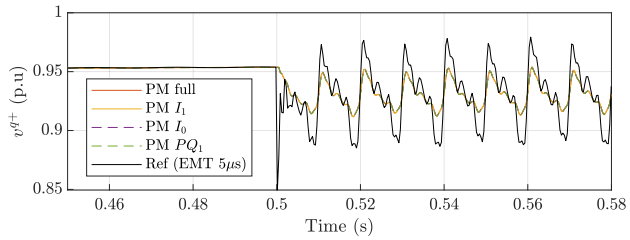

FIGURE 17. Test 5 – v^{q+} simulated by each model at 350 μs.

However, for variables with slower dynamics, the error of PM models was smaller, as shown in Fig. 18 and in Fig. 19.

B. CIGRE SYSTEM

A CIGRE benchmark system (European HV transmission system in [32]) composed of four synchronous generators and two VSCs was simulated. Frequency and voltage droops, LVRT and negative sequence control were enabled during all tests.

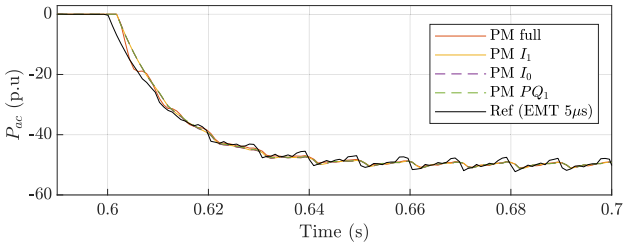

FIGURE 18. Test 5 – P_{ac} simulated by each model at 850 μs.

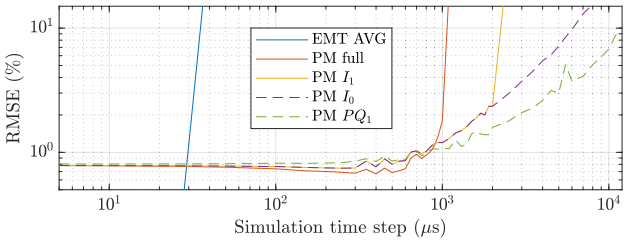

FIGURE 19. Test 5 – P_{ac} setpoint tracking RMSE simulated by each model at several time steps.

1) ASYMMETRICAL FAULT

In this test, an 1 Ω single-phase fault at phase C was applied to bus 2 at $t = 5.0\,s$, lasting for 300 ms. Fig. 20 shows VSC 2 i^{d+} simulated at 850 μs.

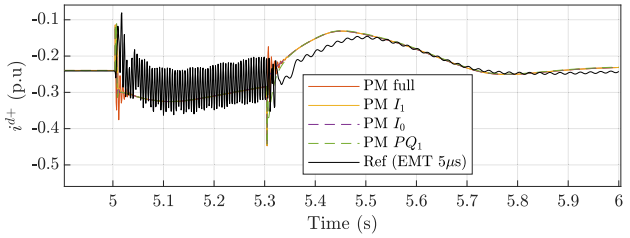

FIGURE 20. Test 1 large system – i^{d+} simulated by each model at 850 μs.

As can be observed in Fig. 20, the PM models assume an average value in relation to the EMT simulation during the transient, and the difference between them reduces 300 ms after the end of the fault. In the CIGRE system, more elements and controllers interact through long transmission lines, which increase the transient response and wider the difference between EMT and PM models. However, even for the CIGRE system, the PM models were still able to track the average value of the EMT simulation. However, the fastest dynamics in the system are still the bottleneck to increasing the simulation time step. As shown in Fig. 21, after the time step increases beyond 1 ms the PM models error increased dramatically. This 1 ms boundary was due to the generators exciter transducer filter time constant, which was exactly 1 ms, and also due to the converters current control time constant that was 1.18 ms.

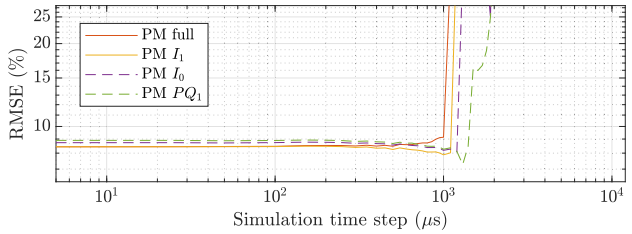

FIGURE 21. Test 1 CIGRE system – i^{d+} RMSE simulated by each model at several time steps.

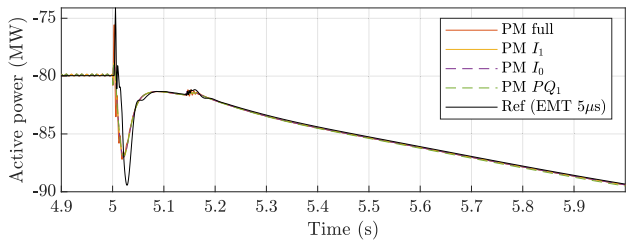

FIGURE 22. Test 2 CIGRE system – VSC 1 P_{ac} simulated by each model at 750 μs.

2) LOSS OF GENERATION

In this test, the generator G1 is disconnected from the system at $t = 5.0\,s$, producing a slow but large transient in the system.

As the transient was electromechanical and did not affect the voltage significantly, the converter's PLLs remained synchronized, and the difference between PM and EMT models was observable only for about 100 ms, as shown in Fig. 22 and Fig. 23.

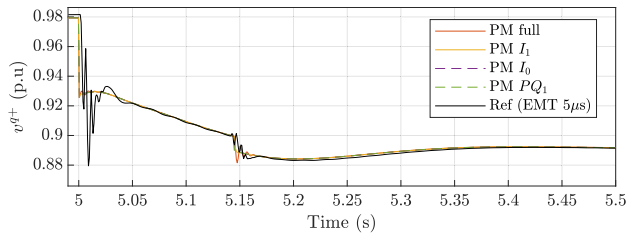

FIGURE 23. Test 2 CIGRE system – VSC 1 v^{q+} simulated by each model at 850 μs.

3) LINE OUTAGE

In this test, a permanent 1 Ω single-phase fault at phase C was applied to the line connecting bus 1 to bus 3. The line was isolated by two circuit breakers, that opened 200 ms and 250 ms after the fault, respectively, producing a transient in the system.

After each transient (fault, first breaker opening and second breaker opening) it is possible to observe in Fig. 24 and Fig. 25 that the difference between EMT and most PM models was high only for about 30 ms. The same is not true for the most approximated PM PQ_1, which took about 100 ms to match the EMT model after each event.

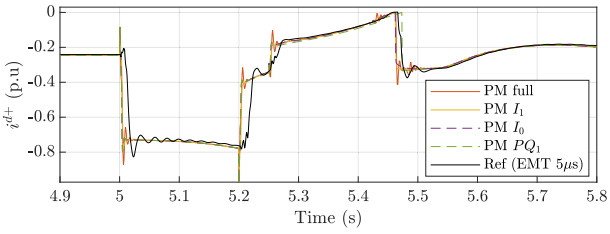

FIGURE 24. Test 3 CIGRE system – VSC 1 i^{d+} simulated by each model at 850 μs.

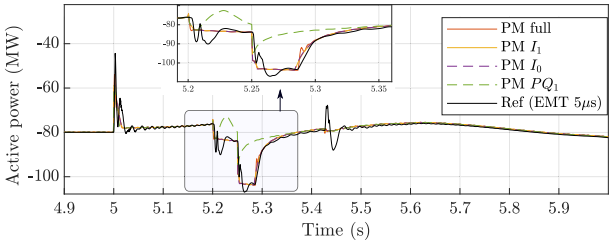

FIGURE 25. Test 3 CIGRE system – VSC 1 P_{ac} simulated by each model at 700 μs.

From the SGs perspective, a small deviation could be observed in the speed (Fig. 26) while the current was precisely tracked after one cycle (Fig. 27).

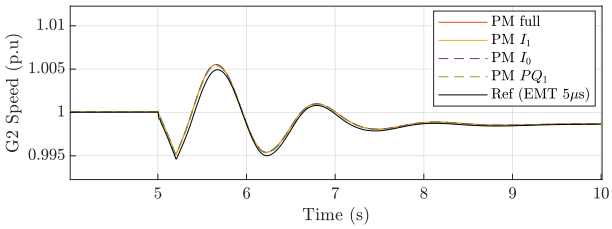

FIGURE 26. Test 3 CIGRE system – SG 3 speed simulated by each model at 750 μs.

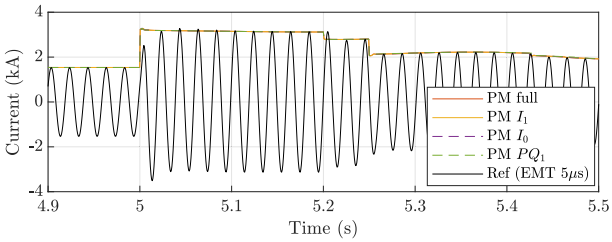

FIGURE 27. Test 3 CIGRE system – SG 2 I_c simulated by each model at 650 μs.

C. ADDITIONAL TESTS

In addition to the tests shown in the previous subsections, further simulations regarding specific tests were performed in more detail and are presented next.

1) PLL DYNAMICS

A growing concern about the PLL dynamics has been observed in recent years as they are often involved

in system instabilities and are commonly overlooked in positive-sequence phasor simulators. Several approaches have been proposed to consider the PLL in phasor simulation (e.g. [33]). This can also be achieved in all phasor models proposed in this paper.

The closed-loop transfer function of the SRF-PLL is

$$C_{pll}(s) = \frac{s\tau_{i,pll} + 1}{s^2/\omega_{pll}^2 + s\tau_{i,pll} + 1} \tag{24}$$

This transfer function can be added to all phasor models presented in this paper, as illustrated in Fig. 28. Using this approach, the angle used by the control in the Park transform is now θ' instead of θ.

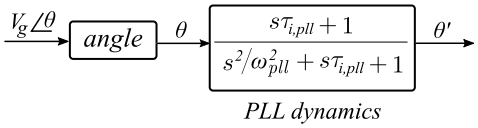

FIGURE 28. PLL closed-loop transfer function used in Phasor simulation.

To confirm the accuracy of (24), a phase jump test was performed both in EMT and in Phasor, and is shown in Fig. 29.

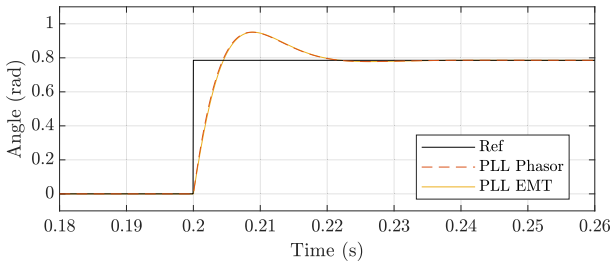

FIGURE 29. PLL tracking a $\pi/4$ phase jump in Phasor and EMT simulation.

As can be observed in Fig. 29, the approach defined in (24) can accurately represent the PLL dynamics.

Although the PLL dynamics can be well represented in phasor simulation, considering these dynamics might not add substantial accuracy in all cases. As it is shown in Fig. 30, for a 5 Ω single-phase fault at phase B between 2.5 and 2.7 s, little difference is observed in the phasor model if the PLL is considered in this test. The same is observed when connecting an additional 150 MW, 20 MVAr load to the system, as shown in Fig. 31 This happens because, as the phasor simulation neglects the grid electrical dynamics, the oscillations seen in the EMT simulation will not exist in phasor, thus these electrical oscillations will not be catch by the equivalent PLL in phasor, even tough its dynamics are well represented.

Several other PLLs, such as filtered PLLs [34], [35], normalized PLLs [36]–[38], among many others [27], may also be represented in the phasor domain using a similar procedure as illustrated in this subsection.

2) LOW SCR

It is often desirable to analyse the converter behaviour in weak-grid conditions, such as with a short-circuit ratio (SCR)

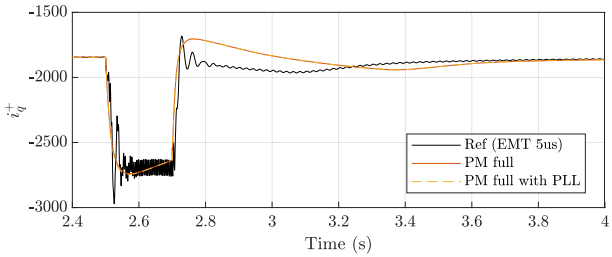

FIGURE 30. Converter current i_q^+ during a single-phase fault. Phasor models with and without equivalent PLL.

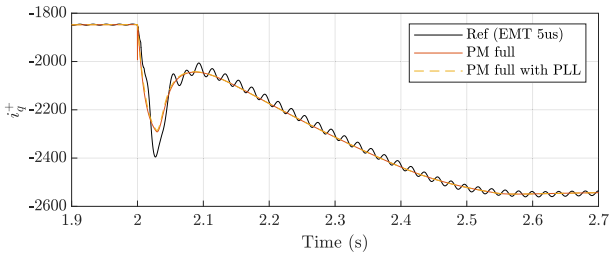

FIGURE 31. Converter current i_q^+ during the connection of a new load. Phasor models with and without equivalent PLL.

lower than 3. In such conditions, phasor models might present an optimistic behaviour as they do not consider electrical oscillations. As an example, for the 50 MW, 30 Mvar setpoint at $t = 0.6$ s and $t = 0.8$ s, respectively (Fig. 32), the converter in EMT starts loosing stability for an SCR below 1.3, while the same converter in phasor model looses stability only below an SCR = 0.86. This value is the same considering or not the equivalent PLL in phasor, shown in the previous subsection. As can be observed in Fig. 32, the EMT AVG model shows the converter in the vicinity of loosing stability, while the phasor model still shows a normal operation.

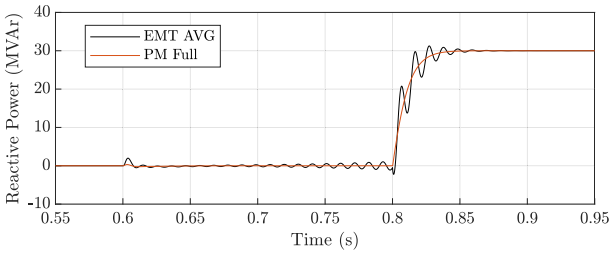

FIGURE 32. Converter reactive power following -30 MVAr setpoint. SCR = 1.3.

VI. DISCUSSION AND GUIDELINES

Based on the tests performed, the following discussion and guidelines follow. They are also summarized in Fig. 33. It is worth mentioning that the events shown in Fig. 33 are only to illustrate the different time scales where each phasor model might be better suitable. The validity of each VSC phasor model can only be confirmed for the tests shown in this paper.

The major advantage of PMs is to increase the simulation time step and reducing the execution time. If a proper

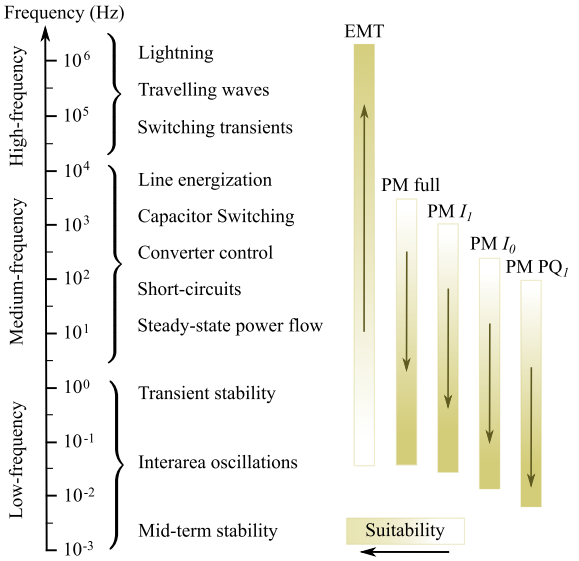

FIGURE 33. Suitability of each model. Frequency ranges are approximated and events are shown only for illustrative purposes. [41], [42].

time step is chosen, the simulation speed can be increased in one or two orders of magnitude (as shown in Fig. 10), transforming hours of simulation in minutes. This allows larger models to be simulated or a higher number of tests to be performed in a feasible time. Another advantage of PMs is a more straightforward interpretation of the results. Analysing current and voltage phasors is more simple than their waveforms. Thus, using PM models can also contribute to increase the level of understanding of the simulation and consequently speed up the post-simulation time, where the analysis and interpretation of the results are performed.

However, one must carefully analyse if the chosen PM is able to represent well the set of studies to be performed. The results presented in the previous sections show that tests involving electromechanical transients and non-solid symmetrical faults are well represented by PM models. However, asymmetrical faults and symmetrical faults that drops voltage near to zero dramatically influence converters' PLLs. As all PM models consider an ideal PLL, their results might be mistakenly optimistic in these cases. The equivalent PLL shown in subsection V-C1 can also be considered, but as the grid's dynamics are not modelled in phasor, they will not be captured by the equivalent PLL, even if it is precisely modelled. In all cases, the PMs took about 100 ms to closely track EMT models (this time vary depending on the system equivalent X/R ratio). Thus, in the simulated systems, transients faster than 100 ms might not be correctly represented by PMs.

Another important aspect to be considered in both EMT and phasor simulation is the choice of the simulation time step. Choosing an arbitrary low time step will lead to an unnecessary slow simulation. Choosing an arbitrary high time step might lead to inaccurate results or numerical instability. Based on the results of the previous section, we recommend that the simulation time step should be between five and ten times smaller than the smallest time constant being simulated (as shown in Fig. 7). In theory, the simulation time step is limited by the Nyquist frequency, which is half of the shortest time constant, but this would be too close from an erroneous simulation. This guideline agrees with past recommendations found in the literature [39], [40]. Based on this guideline, PMs can be even used to perform studies with harmonic content, provided that the greatest harmonic frequency is well represented by the simulation time step (a time step 5 to 10 times smaller than the period of the harmonic of highest magnitude).

Among the PMs discussed in this paper, PM I_1 and I_0 offer the best trade-off between simulation time step and accuracy. Their drawback is that the converter's current control is approximated (PM I_1) or neglected (PM I_0), assuming that the current reference is always correctly tracked. However, if the converter's internal variables are not the focus of the study, these models can significantly increase the simulation speed while providing good precision at the same time.

VII. CONCLUSION

This paper reviewed EMT and phasor models currently used to simulate VSC in grid integration studies. Several modelling guidelines and suitability analyses were provided based on a comprehensive comparative study amongst the models. We addressed a gap related to the suitability of phasor models in studies where the boundary between electromagnetic and electromechanical domains were overlapped. An insightful analysis of the adequate simulation time step for each model and study was provided. The recommendations were based on a systematic comparison amongst the models in several different scenarios.

From the tests performed, it could be observed that the major advantage of PMs is the possibility to increase the simulation time step and reduce the execution time. Another advantage is a more straightforward interpretation of the results when compared to detailed waveforms in EMT. However, the set of studies to be performed by PMs must be carefully analysed. As the PMs consider some idealistic conditions, e.g an ideal PLL, their results might be mistakenly optimistic in cases involving large transients.

The recommendations provided aim to contribute to the discussion about the most suitable models of modern power grids, where the widespread of power electronic interfaced technologies and the reduced inertia are making the grid's dynamic behaviour to become progressively faster.

APPENDIX
TEST SYSTEMS PARAMETERS

The SGs parameters of the CIGRE system are summarized in Table 2. The SG parameters of the small system are equal to G1 in the CIGRE system, but with nominal power equal to 400 MVA. The transmission lines parameters at 50 Hz are: $R_1 = 0.121\ \Omega$/km, $R_0 = 0.446\ \Omega$/km, $L_1 = 1.33$mH/km, $L_0 = 3.73$mH/km, $C_1 = 8.762$ nF/km and $C_0 = 6.373$ nF/km.

TABLE 2. CIGRE system parameters - Synchronous generators.

Parameter	$G0$	$G1$	$G2$	$G3$
S_n (MVA)	1000	700	500	500
V_n (kV)	22.0	22.0	22.0	22.0
X_d (pu)	2.00	1.25	1.667	1.25
X_q (pu)	1.80	1.00	1.125	1.00
X'_q (pu)	0.35	0.333	0.25	0.333
X''_d (pu)	0.25	0.292	0.233	0.292
X''_q (pu)	0.30	0.292	0.225	0.292
X_l (pu)	0.15	0.15	0.15	0.15
R_s (pu)	0.01	0.01	0.01	0.01
T'_{do} (s)	4.485	5.00	6.00	5.00
T''_{do} (s)	0.068	0.002	0.002	0.002
T''_{qo} (s)	0.10	0.002	0.002	0.002
H (s)	6.0	5.0	3.0	5.0

The parameters of the converters are summarized in Table 3. The converter used in the small system has the same parameters as the VSC 1 shown in Table 3.

TABLE 3. Converters parameters.

Parameter	VSC 1	VSC 2
Nominal power S_n (MVA)	100	50
Converter-side voltage V_{n1} (kV)	22	22
Grid-side voltage V_{n2} (kV)	220	220
Transformer leakage reactance X (pu)	0.15	0.15
Transformer resistance R (pu)	0.0037	0.0037
PLL ω_{pll} (rad/s)	$2\pi 80$	$2\pi 80$
Current control ω_c (rad/s)	$2\pi 135$	$2\pi 135$
Power control ω_{pq} (rad/s)	$2\pi 13.5$	$2\pi 13.5$
Frequency droop $k_{droop,f}$	0.1	0.1
Voltage droop $k_{droop,v}$	0.5	0.5
LVRT k_{lvrt} (s)	-2.25	-2.25
LVRT $v_{g,min}$ (s)	0.5	0.5

REFERENCES

[1] P. Kundur, J. Paserba, V. Ajjarapu, G. Andersson, A. Bose, C. Canizares, N. Hatziargyriou, D. Hill, A. Stankovic, C. Taylor, T. Van Cutsem, and V. Vittal, "Definition and classification of power system stability IEEE/CIGRE joint task force on stability terms and definitions," *IEEE Trans. Power Syst.*, vol. 19, no. 2, pp. 1387–1401, Aug. 2004.

[2] N. Hatziargyriou, J. Milanovic, C. Rahmann, V. Ajjarapu, C. Canizares, I. Erlich, D. Hill, I. Hiskens, I. Kamwa, B. Pal, P. Pourbeik, J. Sanchez-Gasca, A. Stankovic, T. V. Cutsem, V. Vittal, and C. Vournas, "Definition and classification of power system stability revisited & extended," *IEEE Trans. Power Syst.*, vol. 36, no. 4, pp. 3271–3281, Jul. 2021.

[3] S. R. Sanders, J. M. Noworolski, X. Z. Liu, and G. C. Verghese, "Generalized averaging method for power conversion circuits," *IEEE Trans. Power Electron.*, vol. 6, no. 2, pp. 251–259, Apr. 1991.

[4] T. Demiray and G. Andersson, "Simulation of power systems dynamics using dynamic phasor models," in *Proc. 10th Symp. Spec. Electr. Oper. Expansion Planning (SEPOPE)*, May 2006, pp. 1–9.

[5] M. Daryabak, S. Filizadeh, J. Jatskevich, A. Davoudi, M. Saeedifard, V. K. Sood, J. A. Martinez, D. Aliprantis, J. Cano, and A. Mehrizi-Sani, "Modeling of LCC-HVDC systems using dynamic phasors," *IEEE Trans. Power Del.*, vol. 29, no. 4, pp. 1989–1998, Aug. 2014.

[6] G. N. Love and A. R. Wood, "Harmonic state space model of power electronics," in *Proc. 13th Int. Conf. Harmon. Quality Power*, Sep. 2008, pp. 1–6.

[7] J. Arrillaga and N. R. Watson, "The harmonic domain revisited," in *Proc. 13th Int. Conf. Harmon. Quality Power*, Sep. 2008, pp. 1–9.

[8] M. S.-P. Hwang and A. R. Wood, "A new modelling framework for power supply networks with converter based loads and generators—The harmonic state-space," in *Proc. IEEE Int. Conf. Power Syst. Technol. (POWERCON)*, Oct. 2012, pp. 1–6.

[9] M. S.-P. Hwang and A. R. Wood, "Harmonic state-space modelling of a controlled HVdc converter," *Electr. Power Syst. Res.*, vol. 124, pp. 65–73, Jul. 2015.

[10] J. Kwon, X. Wang, F. Blaabjerg, C. L. Bak, V.-S. Sularea, and C. Busca, "Harmonic interaction analysis in a grid-connected converter using harmonic state-space (HSS) modeling," *IEEE Trans. Power Electron.*, vol. 32, no. 9, pp. 6823–6835, Sep. 2017.

[11] D. Shu, H. Yang, and G. He, "A harmonic phasor domain cosimulation method and new insight for harmonic analysis of large-scale VSC-MMC based AC/DC grids," *IEEE Trans. Power Electron.*, vol. 36, no. 4, pp. 3909–3924, Apr. 2021.

[12] F. Milan and Á. O. Manjavacas, "Frequency-dependent model for transient stability analysis," *IEEE Trans. Power Syst.*, vol. 34, no. 1, pp. 806–809, Jan. 2019.

[13] S. D'Arco, J. A. Suul, and J. Beerten, "Configuration and model order selection of frequency-dependent π models for representing DC cables in small-signal eigenvalue analysis of HVDC transmission systems," *IEEE J. Emerg. Sel. Topics Power Electron.*, vol. 9, no. 2, pp. 2410–2426, Apr. 2021.

[14] V. Jalili-Marandi, V. Dinavahi, K. Strunz, J. A. Martinez, and A. Ramirez, "Interfacing techniques for transient stability and electromagnetic transient programs IEEE task force on interfacing techniques for simulation tools," *IEEE Trans. Power Del.*, vol. 24, no. 4, pp. 2385–2395, Oct. 2009.

[15] Y. Zhang, A. M. Gole, W. Wu, B. Zhang, and H. Sun, "Development and analysis of applicability of a hybrid transient simulation platform combining TSA and EMT elements," *IEEE Trans. Power Syst.*, vol. 28, no. 1, pp. 357–366, Feb. 2013.

[16] A. A. V. D. Meer, M. Gibescu, M. A. M. M. V. D. Meijden, W. L. Kling, and J. A. Ferreira, "Advanced hybrid transient stability and EMT simulation for VSC-HVDC systems," *IEEE Trans. Power Del.*, vol. 30, no. 3, pp. 1057–1066, Jun. 2015.

[17] P. Zadkhast, X. Lin, F. Howell, B. Ko, and K. Hur, "Practical challenges in hybrid simulation studies interfacing transient stability and electro-magnetic transient simulations," *Electr. Power Syst. Res.*, vol. 190, Jan. 2021, Art. no. 106596.

[18] S. Cole, J. Beerten, and R. Belmans, "Generalized dynamic VSC MTDC model for power system stability studies," *IEEE Trans. Power Syst.*, vol. 25, no. 3, pp. 1655–1662, Aug. 2010.

[19] B. Berggren, R. Majumder, and N. Johansson, "A generic VSC HVDC primary control structure suitable for stability studies," in *Proc. EPRI HVDC FACTS Conf.*, 2013, pp. 1–8.

[20] N. Trinh, M. Zeller, K. Wuerflinger, and I. Erlich, "Generic model of MMC-VSC-HVDC for interaction study with AC power system," *IEEE Trans. Power Syst.*, vol. 31, no. 1, pp. 27–34, Jan. 2016.

[21] G. De Carne, M. Liserre, M. Langwasser, M. Ndreko, R. Bachmann, R. W. De Doncker, R. Dimitrovski, B. J. Mortimer, A. Neufeld, and F. Rojas, "Which deepness class is suited for modeling power electronics?: A guide for choosing the right model for grid-integration studies," *IEEE Ind. Electron. Mag.*, vol. 13, no. 2, pp. 41–55, Jun. 2019.

[22] M. Paolone, T. Gaunt, X. Guillaud, M. Liserre, S. Meliopoulos, A. Monti, T. Van Cutsem, V. Vittal, and C. Vournas, "Fundamentals of power systems modelling in the presence of converter-interfaced generation," *Electr. Power Syst. Res.*, vol. 189, Dec. 2020, Art. no. 106811.

[23] *Technical Brochure 604: Guide for the Development of Models for HVDC Converters in a HVDC Grid*, CIGRE Working Group B4-57, Paris, France, 2014.

[24] S. S. Khan and E. Tedeschi, "Modeling of MMC for fast and accurate simulation of electromagnetic transients: A review," *Energies*, vol. 10, no. 8, p. 1161, 2017.

[25] W. Lu and B.-T. Ooi, "Optimal acquisition and aggregation of offshore wind power by multiterminal voltage-source HVDC," *IEEE Trans. Power Del.*, vol. 18, no. 1, pp. 201–206, Jan. 2003.

[26] H.-S. Song and K. Nam, "Dual current control scheme for PWM converter under unbalanced input voltage conditions," *IEEE Trans. Ind. Electron.*, vol. 46, no. 5, pp. 953–959, Oct. 1999.

[27] S. Golestan, J. M. Guerrero, and J. C. Vasquez, "Three-phase PLLs: A review of recent advances," *IEEE Trans. Power Electron.*, vol. 32, no. 3, pp. 1894–1907, Mar. 2017.

[28] S.-K. Chung, "A phase tracking system for three phase utility interface inverters," *IEEE Trans. Power Electron.*, vol. 15, no. 3, pp. 431–438, May 2000.
[29] L. Harnefors and H.-P. Nee, "Model-based current control of AC machines using the internal model control method," *IEEE Trans. Ind. Appl.*, vol. 34, no. 1, pp. 133–141, Jan./Feb. 1998.
[30] C. Bajracharya, M. Molinas, J. A. Suul, and T. M. Undeland, "Understanding of tuning techniques of converter controllers for VSC-HVDC," in *Proc. Nordic Workshop Power Ind. Electron. (NORPIE)*, Espoo, Finland, Jun. 2008, pp. 1–8.
[31] J. Svensson, M. Bongiorno, and A. Sannino, "Practical implementation of delayed signal cancellation method for phase-sequence separation," *IEEE Trans. Power Del.*, vol. 22, no. 1, pp. 18–26, Jan. 2007.
[32] *Technical Brochure 575: Benchmark Systems for Network Integration of Renewable and Distributed Energy Resources*, CIGRE Task Force C6-04, Paris, France, 2014.
[33] H. N. V. Pico and B. B. Johnson, "Transient stability assessment of multi-machine multi-converter power systems," *IEEE Trans. Power Syst.*, vol. 34, no. 5, pp. 3504–3514, Sep. 2019.
[34] E. Robles, S. Ceballos, J. Pou, J. L. Martín, J. Zaragoza, and P. Ibañez, "Variable-frequency grid-sequence detector based on a quasi-ideal low-pass filter stage and a phase-locked loop," *IEEE Trans. Power Electron.*, vol. 25, no. 10, pp. 2552–2563, Oct. 2010.
[35] F. Gonzalez-Espin, E. Figueres, and G. Garcera, "An adaptive synchronous-reference-frame phase-locked loop for power quality improvement in a polluted utility grid," *IEEE Trans. Ind. Electron.*, vol. 59, no. 6, pp. 2718–2731, Jun. 2012.
[36] M. Karimi-Ghartemani, "Linear and pseudolinear enhanced phased-locked loop (EPLL) structures," *IEEE Trans. Ind. Electron.*, vol. 61, no. 3, pp. 1464–1474, Mar. 2014.
[37] I. Serban and C. Marinescu, "Control strategy of three-phase battery energy storage systems for frequency support in microgrids and with uninterrupted supply of local loads," *IEEE Trans. Power Electron.*, vol. 29, no. 9, pp. 5010–5020, Sep. 2014.
[38] M. G. Taul, X. Wang, P. Davari, and F. Blaabjerg, "Robust fault ride through of converter-based generation during severe faults with phase jumps," *IEEE Trans. Ind. Appl.*, vol. 56, no. 1, pp. 570–583, Jan. 2020.
[39] H. Dommel, "Digital computer solution of electromagnetic transients in single-and multiphase networks," *IEEE Trans. Power App. Syst.*, vol. PAS-88, no. 4, pp. 388–399, Apr. 1969.
[40] J. C. G. de Siqueira, B. D. Bonatto, J. R. Marti, J. A. Hollman, and H. W. Dommel, "Optimum time step size and maximum simulation time in EMTP-based programs," in *Proc. Power Syst. Comput. Conf.*, Aug. 2014, pp. 1–7.
[41] S. Henschel, "Analysis of electromagnetic and electromechanical power system transients with dynamic phasors," Ph.D. dissertation, Fac. Appl. Sci., Dept. Elect. Comput. Eng., Univ. British Columbia, Vancouver, BC, Canada, 1999.
[42] N. Watson and J. Arrillaga, *Power Systems Electromagnetic Transients Simulation*, 2nd ed. London, U.K.: IET, 2018.

VINÍCIUS A. LACERDA received the B.Sc. and Ph.D. degrees in electrical engineering from the University of São Paulo, São Carlos, Brazil, in 2015 and 2021, respectively. He was a Visiting Researcher at the University of Strathclyde, from 2018 to 2019. He is currently a Postdoctoral Researcher at the Universitat Politècnica de Catalunya (CITCEA-UPC), Spain. His research interests include power systems modeling and simulation, short-circuit analysis, and protection and high-voltage direct current systems.

EDUARDO PRIETO ARAUJO (Senior Member, IEEE) received the degree in industrial engineering from the School of Industrial Engineering of Barcelona (ETSEIB), Technical University of Catalonia (UPC), Barcelona, Spain, in 2011 and the Ph.D. degree in electrical engineering from the UPC, in 2016. He joined CITCEA-UPC Research Group, in 2010, and he is currently a Serra Hunter Lecturer with the Electrical Engineering Department, UPC. Since 2021, he has been a Visiting Professor at the Automatic Control Laboratory, ETH Zurich. His main interests include renewable generation systems, control of power converters for HVDC applications, interaction analysis between converters, and power electronics dominated power systems.

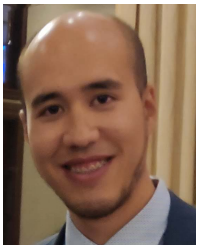

MARC CHEAH-MAÑE (Member, IEEE) received the degree in industrial engineering from the School of Industrial Engineering of Barcelona (ETSEIB), Universitat Politecnica de Catalunya (UPC), Barcelona, Spain, in 2013, and the Ph.D. degree in electrical engineering from Cardiff University, Cardiff, U.K., in 2017. From 2017 to 2020, he was a Research Associate with the CITCEA-UPC, Barcelona. Since March 2020, he has been a Serra Hunter Lecturer at the Electrical Engineering Department, UPC. His research interests include power systems with power electronics, high-voltage direct current systems, and wind and photovoltaic generation.

ORIOL GOMIS-BELLMUNT (Fellow, IEEE) received the degree in industrial engineering from the School of Industrial Engineering of Barcelona (ETSEIB), Technical University of Catalonia (UPC), Barcelona, Spain, in 2001 and the Ph.D. degree in electrical engineering from the UPC, in 2007. In 1999, he joined Engitrol S.L. where he worked as Project Engineer in the automation and control industry. Since 2004, he has been with the Electrical Engineering Department, UPC, where he is currently a Professor and participates with the CITCEA-UPC Research Group. Since 2020, he has been an ICREA Academia Researcher. His research interests include the fields linked with electrical machines, power electronics, and renewable energy integration in power systems.